Received: 27 December 2017 | Revised: 16 July 2018 | Accepted: 1 August 2018

DOI: 10.1002/navi.263

ORIGINAL ARTICLE

WILEY ION

A compact multi-frequency GNSS scintillation model

Charles Rino[1] | Brian Breitsch[1] | Yu Morton[1] | Yu Jiao[2] | Dongyang Xu[3] | Charles Carrano[4]

[1]University of Colorado

[2]Intel Corporation

[3]Colorado State University

[4]Institute for Scientific Research, Boston College

Correspondence
Charles Rino, University of Colorado.
Email: crino@comcast.net

Funding information
AFOSR, Grant/Award Number: FA9550-14-1-0265

Abstract

We present a scintillation model that generates complex scintillation realizations using two-dimensional phase-screen calculations. A compact parameter set simplifies the model. The parameters can be adjusted to reproduce statistically equivalent realizations of target multi-frequency GNSS intensity and phase scintillation time series or defaulted to representative values. Geometric range and TEC inputs can be incorporated to generate realizations of baseband GNSS signals for processor performance evaluation. Selecting model parameters is guided by an efficient encapsulation of the two-dimensional phase-screen theory. Motion of the propagation path through ionospheric structure generates temporal variation. The phase-screen theory incorporates space-to-time conversion via a ratio of the Fresnel scale to an effective scan velocity. A universal strength parameter adjusts the strength of the scintillation.

The model is an encapsulation of results that have been used for GPS performance analysis work that is cited in the paper. A MATLAB implementation of the model with examples has been made available.

1 | INTRODUCTION

In an isolated homogeneous propagation environment, GNSS signal intensity, delay, and phase vary in response to changing satellite-to-receiver range. Propagation through a uniform ionosphere introduces a frequency-dependent complex modulation. Over the bandwidths that supports GNSS waveforms, the result of the ionospheric modulation is a well-known excess group-delay and a corresponding signal phase change. Ionospheric structure induces a stochastic signal amplitude variation and stochastic delay and phase contributions, collectively referred to as scintillation. The ionospheric effects depend on path-integrated total electron content (TEC). The group delay and phase changes are significant errors that must be corrected for precision range measurement. GNSS processors must also accommodate stochastic delay and phase errors. The scintillation error is particularly challenging. Although usually negligible, GNSS scintillation degrades performance and occasionally disrupts the processor operation.

In the absence of noise, biases, and error sources other than scintillation, the signal intensity $I(t;f_c)$, phase $\phi(t;f_c)$, and delay $\tau(t;f_c)$ can be modeled as follows:

$$I(t;f_c) = P(t)|h(t;f_c)|^2, \tag{1}$$

$$\frac{\lambda_c}{2\pi}\phi(t;f_c) = r(t) - cK\cdot TEC(t)/f_c^2 - \frac{\lambda_c}{2\pi}\phi_s(t;f_c), \tag{2}$$

$$c\tau(t;f_c) = r(t) + cK\cdot TEC(t)/f_c^2 + \frac{\lambda_c}{2\pi}\phi_s(t;f_c), \tag{3}$$

where $r(t)$ represents true range, f_c is the carrier frequency, c is the velocity of light in the uniform medium, and $\lambda_c = c/f_c$ is the carrier wavelength. Delay and phase have been scaled to pseudo-range length units. If the total electron content is measured in units of 10^{10} electrons per square meter per meter of path length, the product $cK = 40.3$. The conversion from path-integrated electron content to phase in radians is $\phi(t;f_c) = -2\pi K\bar{N}_e(t)/f_c$, where $K = 1.345\times 10^9\ m^2/s$. The phase scintillation contribution, ϕ_s, has been identified explicitly. The term

$P(t)$ represents path- and aspect-dependent signal intensity variation.

Scintillation intensity and phase are derived from the complex field such that

$$h(t; f_c) = |h(t; f_c)| \exp\{i\phi_s(t; f_c)\}. \tag{4}$$

In the standard model for GNSS delay and error correction, for example, Equations (5.46) and (5.47) in Misra and Enge,[1] the phase scintillation term in (2) and (3) is grouped together with biases and other nuisance factors that must be managed. Additionally, the measured signal phase has a wavelength ambiguity, $M\lambda$, which is removed by estimating a phase offset that aligns pseudo range and $\lambda_c\phi_s(t;f_c)$. Assuming this has been done, the following dual-frequency combination isolates the ionospheric contribution from the geometric contribution $r(t)$:

$$\begin{aligned} &\frac{\phi(t, f_{c_2})/f_{c_2} - \phi(t, f_{c_1})/f_{c_1}}{2\pi K(1/f_{c_1}^2 - 1/f_{c_2}^2)} \\ &= TEC(t) + \frac{\phi_s(t, f_{c_2})/f_{c_2} - \phi_s(t, f_{c_1})/f_{c_1}}{2\pi K(1/f_{c_1}^2 - 1/f_{c_2}^2)}. \end{aligned} \tag{5}$$

The scintillation contribution is an error only to the extent that phase scintillation has a more complicated frequency dependence than the $1/f_c$ dependence associated with path-integrated phase. Under the weak-scintillation conditions that normally prevail for GNSS operations, the frequency dependence of the phase scintillation is indistinguishable from TEC, whereby the error term is properly interpreted as stochastic TEC.

Scintillation-induced performance degradation is highly processor dependent. Moreover, because of the complexity of GNSS processors, simulated signals with injected representative error sources have proven to be the most effective way to evaluate processor performance. A widely used GNSS scintillation model developed by Humphreys et al[2] generates intensity and phase scintillation realizations as a complex autoregressive processes with prescribed spectral content and intensity probability distributions. This modeling approach is attractive because realizations can be generated recursively after initiation with a small number of parameters. However, neither the intensity-phase relations nor the frequency dependence of real GNSS scintillation is preserved. At the time Humphreys et al model was developed, physics-based models that more accurately represent scintillation were deemed too unwieldy for direct modeling application.

Recent results reported by Ghafoori and Skone[3] show that physics-based models can be used effectively for GNSS performance analysis. The GNSS scintillation model introduced in this paper uses a highly efficient implementation of the two-dimensional phase-screen theory described in Carrano and Rino.[4] In the following sections, we summarize the essential results from the two-dimensional phase-screen theory and then derive the efficient GNSS model formulation.

2 | PHASE-SCREEN REALIZATIONS

The proposed GNSS model is formally an algorithm for computing realizations of the stochastic modulation represented by $h(t;f_c)$, which would be referred to as a channel model in communications theory. We start with a spatially varying time-harmonic field propagating from the GNSS source to a receiver.

The propagation of electromagnetic waves in transparent media, such as Earth's ionosphere and atmosphere, is governed by the parabolic wave equation (PWE). Variants of the PWE are quite general, but at GNSS frequencies the scalar form of the PWE is sufficient. We let $\psi(x,y)$ represent a principal component of the electromagnetic field propagating from a GNSS source to a GNSS receiver. The following form of the PWE characterizes the complex modulation imparted to a reference plane wave propagating over the source-to-receiver path:

$$\frac{\partial\psi(x,y)}{\partial x} = \Theta_{\rho_F}\psi(x,y) + ik\Delta n(x,y)\psi(x,y), \tag{6}$$

where $k = 2\pi f_c/c$, $\Delta n(x,y)$ is the local perturbation to the refractive index,

$$\Theta_{\rho_F}\psi(x,y) = \int \Psi(x;q_y)\exp\{-i(q_y\rho_F)^2/2\}\exp\{iyq_y\}\frac{dq_y}{2\pi}, \tag{7}$$

$$\Psi(x;q_y) = \int \psi(x,y)\exp\{-iq_y y\}dy \tag{8}$$

is the Fourier decomposition of the field at x,

$$\rho_F = \sqrt{\Delta x/k} \tag{9}$$

is the Fresnel scale for the propagation distance Δx, and q_y is the spatial frequency in radians per meter.

The first term in the PWE characterizes free-space propagation. The second term in the PWE characterizes the interaction of the field with the propagation medium. With plane-wave initiation, the average intensity of $\psi(x,y)$ is conserved. Path loss and antenna gain variations are incorporated in the $P(t)$ term in (1). In the GNSS frequency range,

$$k\Delta n(x,y) = -cr_e\Delta N_e(x,y)/f_c, \tag{10}$$

where $r_e = 2.8179403 \times 10^{-15}$ m. In the absence of diffraction, the PWE admits a solution of the form

$$\psi(x+\Delta x, y) = \psi(x,y)\exp\left\{ik\int_x^{x+\Delta x}\Delta n(\eta,y)d\eta\right\}. \tag{11}$$

In the absence of refractive-index structure, the propagation term advances the field over the distance Δx. The split-step integration method alternates phase-perturbation and propagation operations. However, experience has shown that intensity fluctuations develop gradually. This has led to replacing the interaction with the structure medium by a single *equivalent* phase screen. With an adjustment to the propagation distance, the propagation operator maps the phase perturbation forward to an observation plane at x.

The procedure for generating a representative phase-screen realization follows from the relation

$$\Delta\phi(y) = \frac{-2\pi r_e}{k}\int_0^l \Delta N_e(\eta, y)d\eta, \tag{12}$$

where l is the path-distance within the structured region. If $\Delta N_e(\eta, y)$ is a homogeneous stochastic process with autocorrelation function $R_{\Delta N_e}(\delta\eta, \delta y)$, the phase autocorrelation function can be computed as

$$R_{\Delta\phi}(\delta y) = \frac{4\pi^2 r_e^2}{k^2} l\int_{-l}^{l}(1 - |\delta\eta|/l)R_{\Delta N_e}(\delta\eta, \delta y)d\delta\eta. \tag{13}$$

The quantity of primary interest is the measurable one-dimensional spectral density function (SDF)

$$\Phi_{\Delta\phi}\left(q_y\right) = \frac{4\pi^2 r_e^2}{k^2} l\int \frac{\sin^2(q_x l/2)}{(q_x l/2)^2}\Phi_{\Delta N_e}\left(q_x, q_y\right)\right)\frac{dq_x}{2\pi}, \tag{14}$$

where $\Phi_{\Delta N_e}\left(q_x, q_y\right)$ is the two-dimensional SDF of the electron density. If l is sufficiently large, the only contribution to (14) comes from $q_x = 0$, which leads to the relation

$$\Phi_{\Delta\phi}\left(q_y\right) \simeq \frac{4\pi^2 r_e^2}{k^2} l\Phi_{\Delta N_e}(0, q_y). \tag{15}$$

If l is smaller than any contributing scale,

$$\Phi_{\Delta\phi}(q_y) \simeq \frac{4\pi^2 r_e^2}{k^2} l\int \Phi_{\Delta N_e}(q_x, q_y)\frac{dq_x}{2\pi}. \tag{16}$$

The integral in Equation 16 represents the one-dimensional in situ SDF. It is noteworthy that the statistical theory of scintillation requires the large-l limit, which equates the phase power-law index with the two-dimensional in situ plasma density index. The equivalent-phase-screen model makes no a priori assumption about how the imposed phase structure is related to in situ structure.

To complete the scintillation model $\Phi_{\Delta\phi}(q_y)$ must be specified. Following Carrano and Rino,[4] we hypothesize a two-component power-law model with the implicit assumption that specifying the defining parameters compensates for the relation between the one-dimensional phase SDF and the path-integrated in situ electron density SDF. Formally,

$$\Phi_{\Delta\phi}(q_y) = C_p\begin{cases} q_y^{-p_1} & \text{for } q_y \le q_0 \\ q_0^{p_2-p_1}q_y^{-p_2} & \text{for } q_y > q_0 \end{cases}, \tag{17}$$

where q_0 is the spatial frequency at which the power-law index changes from p_1 to p_2, and

$$C_p = \frac{4\pi^2 r_e^2}{k^2}[lC1]. \tag{18}$$

The meaning of the $[lC1]$ parameter will be discussed in a later section.

Further, simplification is achieved by scaling spatial wavenumber such that

$$\mu = q\rho_F. \tag{19}$$

In scaled spatial wavenumber units the stochastic path-integrated-phase component is defined by the two-component SDF $P_{\Delta\phi}(\mu) = \Phi_{\Delta\phi}(q_y\rho_F)/\rho_F$, where

$$P_{\Delta\phi}(\mu) = C_{pp}\begin{cases} \mu^{-p_1} & \text{for } \mu_0 \ge 1 \\ \mu_0^{p_2-p_1}\mu^{-p_2} & \text{for } \mu_0 < 1 \end{cases}, \tag{20}$$

and

$$C_{pp} = (C_p\rho_F^{p_1-1}). \tag{21}$$

Phase realizations are generated by imposing the desired phase SDF on white noise. Formally,

$$\overline{\phi}_k = \sum_{n=0}^{N-1}\sqrt{P_{\Delta\phi}\left(n\Delta\mu\right)\Delta\mu/\left(2\pi\right)}\eta_n\exp\{-2\pi ink/N\}, \tag{22}$$

where η_n is a zero-mean random process with the Hermitian property $\eta_n = \text{mod}(\eta_N^*, N)$ and the white-noise property

$$\left\langle\eta_n\eta_{n'}^*\right\rangle = \delta_{n-n'}. \tag{23}$$

The form of (22) and the white-noise property of η_n ensures that $\overline{\phi}_k$ has the prescribed SDF. Propagation from the phase screen to the observation plane is generated with the following pair of discrete Fourier transformations:

$$\Psi(0; n\Delta\mu) = \sum_{k=0}^{N-1}\exp\{i\overline{\phi}_k\}\exp\{-2\pi ink/N\}, \tag{24}$$

$$\psi\left(\rho_F; k\Delta y/\rho_F\right) = \frac{1}{N}\sum_{n=0}^{N-1}\Psi(0; n\Delta\mu)\exp\left\{-i(n\Delta\mu)^2/2\right\} \times\exp\{2\pi ink/N\}. \tag{25}$$

In normalized units, (24) and (25) do not depend on ρ_F. Functionally, the Fresnel scale determines the distance from the phase screen at which the predicted intensity scintillation will be observed. The same structure would be observed at distances and frequencies that have the same Fresnel scale.

Signal parameter measurements are reported as time series sampled at an interval Δt. Space-to-time conversion involves the true Doppler offset contributed by the range rate, the TEC variation, and the relative motion of

the structure in the phase-screen reference frame. This last component is modeled by an effective scan velocity, v_{eff}, such that $y = v_{\text{eff}}t$. The signal model defined by (3) and (2) introduced the range and TEC variations explicitly. The scintillation-induced Doppler comes from $\phi_s(t)$. The conversion from spatial wavenumber to the Doppler frequency offset from the center frequency is $f_D = q.v_{\text{eff}}/(2\pi)$. This leads to the following relation between the normalized spatial wavenumber and f_D:

$$\mu = 2\pi f_D\,(\rho_F/v_{\text{eff}})\,. \tag{26}$$

For a data set with N samples, the periodogram Doppler frequency span is $-N/(2\Delta t)$ to $(N-1)/(2\Delta t)$. A sampled phase screen constructed with

$$P(\mu_n)2\pi\Delta f_D/\Delta\mu = P(\mu_n)\rho_F/v_{\text{eff}} \tag{27}$$

where $\Delta f_D = 1/(N\Delta t)$ will generate a statistically equivalent realization of the time-varying scintillation defined by the phase-screen structure. At that point the complex field realization is the desired channel model $h(t;f_C)$.

3 | PHASE SCREEN THEORY

The statistical theory of scintillation characterizes measurable coherence properties in terms of a statistical characterization of the structure. The two-dimensional theory admits a complete analytic characterization. From Carrano and Rino,[4] the intensity SDF can be computed as follows:

$$I(\mu) = 2\int_0^\infty \exp\{-\gamma(\eta,\mu)\}\cos(\eta\mu)\,d\eta, \tag{28}$$

where

$$\gamma(\eta,\mu) = 16\int_0^\infty P(\chi)\sin^2(\chi\eta/2)\sin^2(\chi\mu/2)\frac{d\chi}{2\pi}. \tag{29}$$

Carrano and Rino[4] developed a highly efficient algorithm for evaluating $I(\mu)$ as a function of the universal strength parameter

$$U = C_{pp}\begin{cases} 1 & \text{for } \mu_0 \geq 1 \\ \mu_0^{p_2-p_1} & \text{for } \mu_0 < 1 \end{cases}, \tag{30}$$

and p_1, p_2, and μ_0.

The universal strength parameter U orders the scintillation strength such that $U > 1$ corresponds to strong scatter with $S4$ approaching or exceeding unity, and $U < 1$ corresponds to weaker scatter with $S4 < 1$. Note that U, p_1, μ_0, and p_2 determine C_{pp}. For modeling U, this is more convenient because it relates directly to scattering strength. Carrano's algorithm also computes $S4$, which is formally defined by the integral

$$S4^2 = 2\int_0^\infty I\,(\mu)\,d\mu/\,(2\pi)\,. \tag{31}$$

The Fourier transform of $I(\mu)$ generates the intensity autocorrelation function, which measures the intensity decorrelation time.

Space-to-time conversion has already been introduced. The Doppler frequency range scales via ρ_F/v_{eff} in (26) to a subrange of μ. In effect, ρ_F/v_{eff} is a scale factor that adjusts the measured Doppler range to match the normalized theoretical variation.

4 | MODEL PARAMETER SPECIFICATION

Generating a scintillation model that proceeds from a structure model requires knowledge of the propagation path geometry, the magnetic field direction, the location of the structure along the propagation path, and its drift rate.[5] The phase-screen model is parameterized in such a way that the complete specification is unnecessary for generating representative intensity and phase realization. However, the connections to structure models ultimately validates the model. The critical parameter is C_p, which establishes the disturbance level. The phase-screen development (18) is driven by a scale parameter, $[lC1]$, which absorbs the relation between the path-integrated phase and the one-dimensional in situ turbulent strength.

A three-dimensional turbulent strength parameter is used in the WBMOD global scintillation model,[6] which incorporates an empirically derived scaling that imposes solar cycle, seasonal, diurnal, and geographic dependencies. The three-dimensional and one-dimensional turbulence strengths are related in such a way that $[lC1]$ can be extracted from the WBMOD formulation. Moreover, the WBMOD computation of $S4$ is the weak-scatter limit of the three-dimensional form of (28). The two-dimensional propagation model is restricted to propagation geometries that exclude near-field-aligned propagation paths. The three-dimensional WBMOD model is not restricted, but the structure characteristics as field-aligned propagation is approached should be used guardedly.

To illustrate the use of normalized parameters consider the theoretical prediction of the PSD of the intensity time series

$$\Phi_I(f_D)/(2\pi[\rho_F/v_{eff}]) = I(\mu), \tag{32}$$

where $\Phi_I(f_D)$ is the intensity PSD. The ratio $[\rho_F/v_{eff}]$, which absorbs the geometrical dependence, is placed in square brackets to emphasize that it can be treated as a single scale parameter that determines the Doppler mapping to the defining scale-free wavenumber μ. Whereas irregularity parameter estimation (IPE) as described in

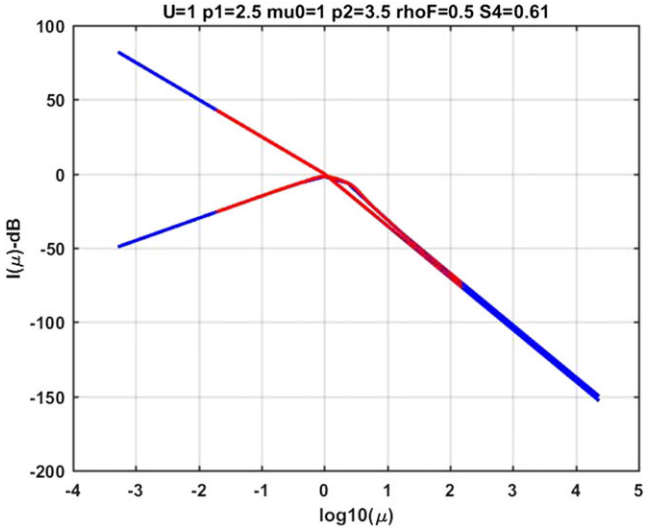

FIGURE 1 Theoretical calculation of phase and intensity SDFs in normalized spatial-frequency units. Blue curve is full range. Red curve is subrange determined by ρ_F/v_{eff}. [Color figure can be viewed at wileyonlinelibrary.com]

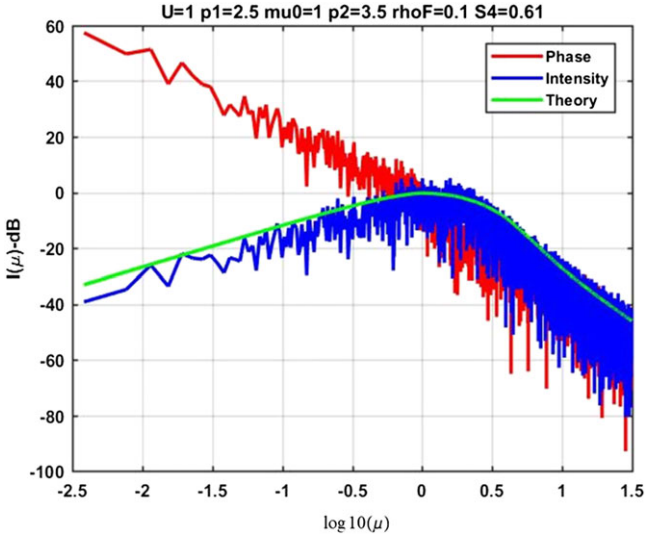

FIGURE 2 Phase (red) and intensity (blue) PDFs from phase-screen realization. [Color figure can be viewed at wileyonlinelibrary.com]

Carrano and Rino[4,7] estimates the defining parameters, a scintillation model specifies the expected range of C_p, the spectral index, and the break-scale.

For performance evaluation one is interested mainly in the severity and structure of scintillation that might be expected. Specifying $U \geq 1$ at the GPS L1 frequency, generates extreme conditions that would be expected only for highly disturbed nighttime equatorial paths. The two-component inverse power-law model itself has only been associated with such highly disturbed equatorial structure.[8] At the time of writing of this paper only the PBMOD model[9] incorporates a two-component power-law model.

A representative model for L-Band GNSS scintillation can be realized by assigning p_1 and p_2 values with $\mu_0 = 1$ for $U \geq 1$. Setting $\mu_0 = 1$ aligns the break scale with the Fresnel scale, which is a reasonable approximation. For $U < 1$ a single represented power-law index can be assigned. Note that for the single power law and $\mu_0 = 1$ models, $U = C_p \rho_F^{(p_1-1)}$. Figure 1 shows the theoretical calculation of $P(\mu)$ from (20) and $I(\mu)$ from (28) for the parameters shown in the figure title. The blue curves are computed over a μ range that captures all of the significant intensity SDF content. The red curves capture the Doppler range determined by $[\rho_F/v_{\text{eff}}]$ and the sample rate. The largest contributing frequency is half the Nyquist frequency. The smallest contributing Doppler frequency is the frequency resolution. The scale factor $[\rho_F/v_{\text{eff}}]$ cannot be chosen arbitrarily. As a check on sampling adequacy, integrating the intensity PSD over the frequency subrange should reproduce the theoretical $S4$ value to within 10% of its full-range value.

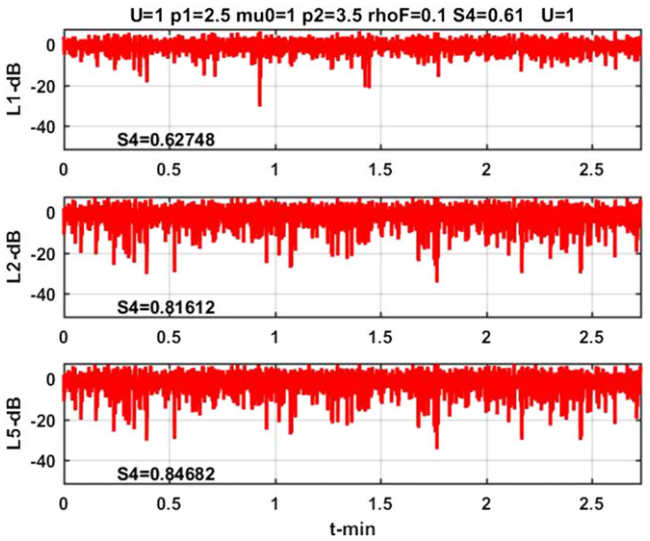

FIGURE 3 GPS L1, L2, and L5 Intensity realizations. [Color figure can be viewed at wileyonlinelibrary.com]

Figure 2 shows the measured intensity and phase PSDs extracted from the complex signal realization. The theoretical prediction of the intensity SDF is overlaid (green). The PSD of the phase derived from the complex signal realization is also shown (red). Both theory and observation confirm that the high-frequency range of the intensity SDF reproduces the weak-scatter limit. Under weak-scatter conditions, the phase SDF follows the same frequency dependence but offset by 6 dB. The scale in Figure 1 was set to show the large dynamic range. The offset is difficult to see.

Figure 3 shows intensity realizations for the GPS L1, L2, and L5 frequencies. The figure title lists the initiating

parameters for the L1 phase-screen. The L2 and L5 realizations use the same phase structure scaled to the L2 and L5 frequencies with $C_{pp} \sim f_c^{2+(p_1-1)/2}$ and $\rho_F \sim f_c^{1/2}$. The L2 and L5 frequencies are 51 MHz apart, which reflects a measurable but small structure change. The coherence time can be varied by changing $[\rho_F/v_{\text{eff}}]$ within the limits that capture defining range of the intensity PSD. These limits are real constraints in that they establish sampling adequacy.

5 | CONCLUSIONS

We have developed and demonstrated a GNSS scintillation model for generating multi-frequency realizations of complex scintillation. As described in the previous section, the model is defined by two parameters, namely the universal scintillation parameter U and the scale parameter $[\rho_F/v_{\text{eff}}]$, which completely absorbs the geometrical dependence of scintillation. We note that both ρ_F and v_{eff} can be computed from three-dimensional models. Indeed, it has been demonstrated that IPE estimates of the ratio parameter can be used to estimate the propagation distance if v_{eff} or drift velocity if the geometry is known.[4,7] However, caution should be used in interpreting near zero values of v_{eff}, which can occur for propagation paths within the meridian plane.

The model itself provides guidelines for interpreting GNSS scintillation data (see Appendix A for Model Usage). The procedure used for generating statistical realizations of the initiating phase-screen structure cannot be used reliably for generating realizations of the actual phase or intensity structure. This can be seen most directly by comparing the intensity and phase structure. Figure 4 is a zoomed view of the L5 intensity and phase structure at the deepest fade between 1 and 2 min. The result can be compared to Figure 2 in Humphreys et al,[10] which shows measured associations of deep L1 fades and rapid phase changes. The simulated data are noise-free, which means that the phase change can be fully resolved.

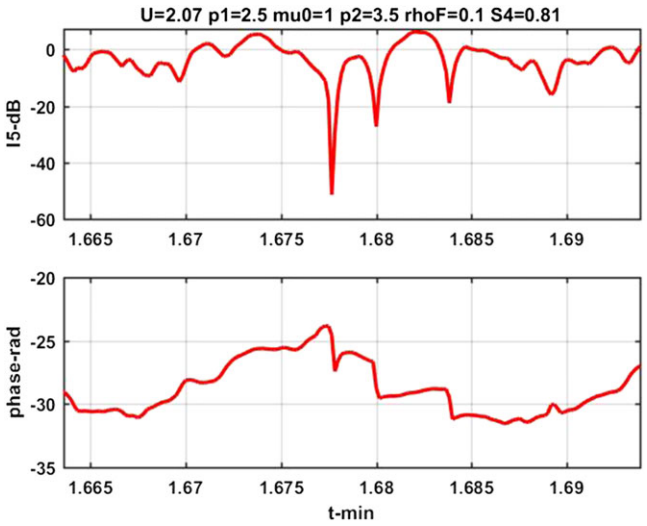

FIGURE 4 Zoom view of intensity and phase at deepest L5 fade between 1.5 and 2 min. [Color figure can be viewed at wileyonlinelibrary.com]

A discussion of the relation of phase-screen mode to multi-frequency measurements and moving platforms can be found in Jiao et al,[11,12] respectively. A discussion of the geometrical dependence can be found in Jiao et al.[13]

ORCID

Charles Rino http://orcid.org/0000-0003-2560-0478
Yu Morton http://orcid.org/0000-0001-9173-2888

REFERENCES

1. Misra P, Enge P. *Global Positioning System Signals, Measurements, and Performance*. Lincoln, MA: Ganga-Jamuna Press; 2012.
2. Humphreys TE, Psiaki ML, Hinks CJ, O'Hanlon B, Kintner PM Jr. Simulating ionosphere-induced scintillation for testing GPS receiver phase tracking loops. *IEEE J Sel Top Sign Process*. 2009;3(4):707-715.
3. Ghafoori F, Skone S. Impact of equatorial ionospheric irregularities on GNSS receivers using real and synthetic scintillation signals. *Radio Sci*. 2015;50:294-317.
4. Carrano CS, Rino CL. A theory of scintillation for two-component power law irregularity spectra: overview and numerical results. *Radio Sci*. 2016;51:789-813.
5. Beniguel Y. Global ionospheric propagation model (GIM): a propagation model for scintillations of transmitted signals. *Radio Sci*. 2002;37:4026-4043.
6. Secan JA, Bussey RM, Fremouw EJ, Basu S. An improved model of equatorial scintillation. *Radio Sci*. 1995;30(3):607-617.
7. Carrano CS, Rino CL, Groves KM. Maximum likelihood estimation of phase screen parameters from ionospheric scintillation spectra. Proceedings of the 15th International Ionospheric Effects Symposium; 2017; Alexandria, VA, 1-11.
8. Rino CL, Groves KM, Carrano CS, Roddy PA. A characterization of intermediate-scale spread f structure from four years of high-resolution C/NOFS satellite data. *Radio Sci*. 2016;51:779-788.
9. Retterer JM. Forecasting low latitude radio scintillation with 3-D iionospheric plume models: 2. Scintillation calculation. *J Geophys Res*. 2010;115:A03306.
10. Humphreys TE, Psiaki ML, Ledvina BM, Cerruti AP, Kintner PMJr. Data-driven testbed for evaluating GPS carrier tracking loops in ionospheric scintillation. *IEEE Trans Aerosp Electron Syst*. 2010;46(4):707-715.
11. Jiao Y, Xu D, Rino C, Morton Y, Carrano C. A multi-frequency GPS signal strong equatorial ionospheric scintillation simulator: algorithm, performance, and characterization. *IEEE Trans Aerosp Electron Syst*. August 2018;54(4):1947-1965.
12. Jiao Y, Rino C, Morton Y. Ionospheric scintillation simulation on equatorial GPS signals for dynamic platforms. *J Inst Navig*. 2018;65:263-274. https://doi.org/10.1002/navi.231

13. Jiao Y, Xu D, Morton YT, Rino C. Equatorial scintillation amplitude fading characteristics across the GPS frequency bands. *NAVIGATION*. Fall 2016;63(3):267-281.

How to cite this article: Rino C, Breitsch B, Morton Y, Jiao Y, Xu D, Carrano C. A compact multi-frequency GNSS scintillation model. *NAVIGATION*. 2018;1–7. https://doi.org/10.1002/navi.263

APPENDIX A: MODEL USAGE

As a guide to the use of the model, we assume that a user is interested in simulating sampled multi-frequency GNSS complex scintillation realizations. Real intensity data are typically reported in normalized intensity units, denoted $CN0(k\Delta t; f_l)$, where f_l is the GNSS frequency. A detrending operation is performed by estimating a local mean, denoted $\bar{I}(\Delta t; f_l)$, and normalizing the intensity. The model characterizes the detrended intensity

$$I_k^l = CN0(k\Delta t; f_l)/\bar{I}(\Delta t; f_l), \tag{1}$$

which has a constant unity mean over segments comprised of N samples. It is important to choose a detrend interval large enough to capture the low-frequency content. A periodogram provides estimates of power spectral density at the Doppler frequencies

$$2/(N\Delta t) \le n/(N\Delta t) \le 1/\Delta t, \tag{2}$$

for $1 \le n \le N$. Because the intensity scintillation is intrinsically high-pass filtered, no windowing is needed. Moreover, windowing biases the estimate and distorts the critical low-frequency content. Regarding background noise, the contributing Doppler range for analysis can be truncated.

Reiterating, model applications start with a specification of the sample interval Δt and the number of samples, which determines a segment length $N\Delta t$. A periodogram estimate or calculation generates $\Phi(n\Delta f_D)$, where $\Delta f_D = 1/(N\Delta t)$ is the Doppler sampling interval. From (26), Doppler frequency can be converted to normalize spatial frequency μ, but ρ_f/v_{eff} is unknown. However, $I(\mu)$ as defined by (28), (29), and (30) is completely specified by U, C_{pp}, p_1, μ_0, and p_2, whereas IPE adjusts the defining parameters and ρ_f/v_{eff}. In the section on Model Parameter Selection, we suggested using fixed representative values such as $p_1 = p_2 = 2.7$ or $p_1 = 1.5$, $p_2 = 3$, and $\mu_0 = 1$. At that point, model calculations of S_4 can be used to determine the value of U that reproduces S_4 at a target frequency. The final step adjusts ρ_f/v_{eff} to center or match the Doppler range to the central μ range as illustrated in Figure 1.

At that point C_{pp} can be extracted from (30). The phase spectrum in Doppler units can then be constructed from (26) and (27). With the Doppler spectrum defined at the reference frequency, multiple-frequency complex signal realizations can be computed from (24).

The sequence of operations just described proceeds from a sample frequency, a duration, and an $S4$ specification at a target frequency to realizations at the target frequency and other specified frequencies. No specification of the actual propagation geometry and penetration point motion are needed. However, if the geometry and drift parameters are known, the information can be used to estimate the propagation distance from the structure or the structure drift. A MATLAB implementation of the GNSS model with examples can be downloaded from `https://github.com/cu-sense-lab/gnss-scintillation-simulator`.